Forty Postmortem Examinations in COVID-19 Patients

Two Distinct Pathologic Phenotypes and Correlation With Clinical and Radiologic Findings

Simona De Michele, MD,[1,] Yu Sun, MD, PhD,[1,*] Mine M. Yilmaz, MD,[1,*] Igor Katsyv, MD, PhD,[1] Mary Salvatore, MD,[2] Amy L. Dzierba, PharmD,[3] Charles C. Marboe, MD,[1] Daniel Brodie, MD,[4] Nina M. Patel, MD,[4] Christine K. Garcia, MD, PhD,[4] and Anjali Saqi, MD, MBA[1]*

From the [1]Department of Pathology and Cell Biology, [2]Department of Radiology, [3]Department of Pharmacy, and [4]Division of Pulmonary, Allergy and Critical Care Medicine, Department of Medicine, Columbia University Irving Medical Center and the NewYork-Presbyterian Hospital, New York, NY.

Key Words: COVID-19 pulmonary pathology; COVID-19 lung phenotypes; COVID-19 autopsy series; Pulmonary pathology; Coronavirus

Am J Clin Pathol 2020;XX:1–14

DOI: 10.1093/AJCP/AQAA156

ABSTRACT

Objectives: *Although diffuse alveolar damage, a subtype of acute lung injury (ALI), is the most common microscopic pattern in coronavirus disease 2019 (COVID-19), other pathologic patterns have been described. The aim of the study was to review autopsies from COVID-19 decedents to evaluate the spectrum of pathology and correlate the results with clinical, laboratory, and radiologic findings.*

Methods: *A comprehensive and quantitative review from 40 postmortem examinations was performed. The microscopic patterns were categorized as follows: "major" when present in more than 50% of cases and "novel" if rarely or not previously described and unexpected clinically.*

Results: *Three major pulmonary patterns were identified: ALI in 29 (73%) of 40, intravascular fibrin or platelet-rich aggregates (IFPAs) in 36 (90%) of 40, and vascular congestion and hemangiomatosis-like change (VCHL) in 20 (50%) of 40. The absence of ALI (non-ALI) was novel and seen in 11 (27%) of 40. Compared with ALI decedents, those with non-ALI had a shorter hospitalization course (*P = *.02), chest radiographs with no or minimal consolidation (*P = *.01), and no pathologically confirmed cause of death (9/11). All non-ALI had VCHL and IFPAs, and clinically most had cardiac arrest.*

Conclusions: *Two distinct pulmonary phenotypic patterns—ALI and non-ALI—were noted. Non-ALI represents a rarely described phenotype. The cause of death in non-ALI is most likely COVID-19 related but requires additional corroboration.*

Key Points

- This study evaluates the spectrum of pulmonary pathology in a cohort of 40 decedents with reverse transcription polymerase chain reaction–confirmed severe acute respiratory syndrome coronavirus 2.
- Three major pulmonary patterns were identified: acute lung injury (ALI), intravascular fibrin or platelet-rich aggregates, and vascular congestion and hemagiomatosis-like change (VCHL). Furthermore, there was a cohort without ALI, which suggested two main pulmonary pathologic phenotypes—ALI and non-ALI.
- Coronavirus disease 2019 (COVID-19) presents with ALI or non-ALI phenotypes. COVID-19 may have pulmonary, cardiac, and/or vascular manifestations.

Coronavirus disease 2019 (COVID-19) is widespread globally, yet there are relatively limited data on its underlying pulmonary pathology. COVID-19 pathology has been described only in limited case reports and mostly small case series.[1-16] Overall, these comprise a combination of surgical resections, complete autopsies, or postmortem biopsy sampling.

The most commonly described pathology is acute lung injury (ALI) with hyaline membranes consistent with diffuse alveolar damage (DAD), which corresponds

clinically to acute respiratory distress syndrome (ARDS). In a minority of cases, DAD was absent, and organizing pneumonia,[4] chronic inflammation, congestion,[6,8,9] and bronchopneumonia[12] were present. Fibrin deposition[4,10,11] or microthrombi[5,12-14] have also been described, most often in conjunction with DAD.

While the current literature indicates that ALI is the primary pulmonary pathology in patients with COVID-19, it also suggests that some patients may have multiple additional or concurrent pathologic manifestations. Which pathologic findings are directly attributable to COVID-19 and which are unrelated remain unclear. A systematic and multidisciplinary approach with correlation among clinical, radiologic, and pathologic findings in a large series may improve our understanding of the spectrum of disease in COVID-19.

The aim of the current study, conducted at an academic teaching hospital in New York City, the epicenter of the pandemic in the United States, is to describe the pulmonary pathology seen in a large series of autopsies from decedents with confirmed severe acute respiratory syndrome coronavirus 2 (SARS-CoV-2) infection based on real-time reverse transcription polymerase chain reaction (RT-PCR) and to correlate the results with imaging, clinical, and laboratory data.

Materials and Methods

Case Selection

Following institutional review board approval, autopsy cases from patients with either premortem or postmortem RT-PCR–confirmed SARS-CoV-2 were reviewed.

Autopsy Procedure

The autopsies of confirmed or suspected COVID-19 cases were performed using the Virchow technique and recommendations provided by the US Centers for Disease Control and Prevention.

Macroscopic Examination

The lungs were serially sectioned, and samples were taken from grossly or radiographically identified abnormal regions. If neither was evident, at minimum one section from each lobe of the lung was taken.

Microscopic Evaluation: Overview

Analyses were performed based on the microscopic pulmonary patterns identified. First, all microscopic patterns were categorized as either "major" or "minor." Second, "novel" pathologic findings were defined as a deviation from the current literature, which describes ALI as the main underlying pulmonary pathologic pattern in COVID-19 and unexpected clinically. Third, "discordant" was characterized as incongruity of microscopic patterns with the radiologic findings.

Microscopic Evaluation: Major vs Minor Patterns

All H&E-stained lung slides were reviewed. A comprehensive list of features, including quantification where appropriate, was generated (Supplemental Table 1; all supplemental materials can be found at *American Journal of Clinical Pathology* online). All slides were evaluated for each of the features, and from these, a case diagnosis was formulated.

Following review of all cases, microscopic patterns were categorized as either "major" or "minor" findings depending upon whether they were present in 50% or more or less than 50% of all cases, respectively. In addition, to qualify as "major," the morphologic features had to be present in more than one slide and encompass 5% or more of the area of all slides with the exception of intravascular fibrin or platelet-rich aggregates (IFPAs), which had to be present in at least one slide. IFPAs were designated as such to reflect their unknown etiology—thrombi vs emboli. The IFPAs were further characterized by their location (including in the pulmonary artery, pulmonary vein, or other small vessels), quantity (including focal [rare vessels] or diffuse [three or more vessels in a single slide]), and size (including large or small). Large IFPAs corresponded to either proximal elastic arteries accompanying airways or veins within interlobular septa.

When performed and available, ancillary tests (histochemical or immunohistochemical stains) were reviewed.

Clinical and Laboratory Data

For each case, the electronic medical record was reviewed for demographics, initial presentation, comorbidities, hospital course, laboratory values, and therapies.

Imaging

All available chest imaging, including chest radiographs and computed tomography (CT) scans, was reviewed. When multiple chest radiographs were performed, the first and last available were graded on a scale of 0 to 3: grade 0, lung with no alveolar opacities; grade 1 (minimal), less than one-third of the lung with alveolar opacities; grade 2 (moderate): one-third to two-thirds of the lung with alveolar opacities; and grade 3 (marked),

DOI: 10.1093/ajcp/aqaa156

more than two-thirds of the 2/3 lung with alveolar opacities. Change of the grade between the first and last chest radiographs was recorded.

Novel and Discordant Findings

Each component—clinical, laboratory data, imaging and pathology—was first reviewed independently by the corresponding subspecialists (pulmonologists who managed patients with COVID-19, a thoracic radiologist, a thoracic pathologist, and pathologists who performed the prosections). Following the microscopic review, the major pulmonary pathology patterns were assessed for novel and discordant findings.

Additional data were obtained, as needed, to adjudicate discordant findings. This included further comprehensive evaluation of clinical, laboratory, and radiologic data as well as the cause of death, which was determined based on macroscopic and microscopic pulmonary and extrapulmonary pathology. Assessment of cardiac findings, performed by a cardiac pathologist (C.C.M.), included but was not limited to evaluation for early or late ischemic changes and myocarditis. In the absence of pathologic evidence, cause of death was established based on adjudication of the clinical and pathologic findings. The cause of death was categorized into major categories: cardiac failure, respiratory failure, cardiorespiratory failure, neurologic (eg, intracranial hemorrhage), sepsis, thromboembolic event, or multiorgan failure. The level of certainty was stratified into definite (identifiable macroscopic and microscopic pathology) and probable (no identifiable macroscopic or microscopic pathology).

Controls

H&E slides from prepandemic, non–COVID-19 postmortem examinations with ALI (n = 7) and non-ALI (n = 7) were reviewed.

Statistical Analyses

To correlate the "major" pathologic, clinical, and laboratory data, Pearson or ϕ correlation coefficients were calculated for all pairwise combinations of clinical, laboratory, radiologic, and major pathologic findings. To account for missing values, all correlations were computed on complete pairwise observations. The statistical significance of differences in the distributions of clinical, laboratory, radiologic, or major pathologic findings between patients with ALI and without ALI was assessed using a two-tailed Wilcoxon rank-sum test for continuous or ordinal variables and a Fisher exact test for binary variables. For all analysis, Holm-adjusted $P < .05$ was considered significant. All statistical analyses were performed in R version 3.6.3 (R Foundation for Statistical Computing).

Results

Forty sequential lung specimens from postmortem examinations of patients infected with SARS-CoV-2 were evaluated. All patients had nasopharyngeal swabs, either premortem (n = 32) or postmortem (n = 8), that confirmed SARS-CoV-2 infection. Complete postmortem examinations, with the exclusion of the head in a few cases, were performed.

Clinical Characteristics and Imaging

Patients ranged in age from 38 to 97 years (median age, 71.5 years) Table 1. The majority were men (70%) and Hispanic or Latino (57.5%). Hypertension was present in 85%, diabetes mellitus in 50%, preexisting heart disease in 38%, and preexisting lung disease in 25%; one or more of these were present in 37 (92.5%) of 40 patients. Twenty-six (65%) patients received supplemental oxygen, and 23 (57.5%) were intubated or received invasive mechanical ventilation. The mean time from admission to death was 10.4 days (range, 0-45 days).

Laboratory data (including platelet count for 33, international normalized ratio on admission for 32, D-dimer for 26, troponin-T for 32, N-terminal prohormone of brain natriuretic peptide for 20, interleukin 6 [IL-6] for 24) were available for a subset of 40 patients. Chest radiographs were available for 32 of 40 patients, 26 had multiple chest radiographs, and three had chest CTs.

Pulmonary Pathology: Major and Minor Microscopic Patterns

Three major pulmonary findings included ALI in 29 (73%) of 40, IFPAs in 36 (90%) of 40, and vascular congestion and hemangiomatosis-like change (VCHL) in 20 (50%) of 40 Figure 1, Image 1, and Image 2. ALI comprised the histologic spectrum of DAD with an acute (exudative) phase demonstrating hyaline membranes with or without an organizing (proliferative) phase exhibiting interstitial fibroblastic proliferation as well as a single case with predominantly fibrin, compatible with acute fibrinous and organizing pneumonia (AFOP). When present, ALI was evident in 33.3% to 100% of H&E slides for each case (mean, 78.4%; median, 85.7%).

VCHL was present in 50% of the cases and characterized by a widening of alveolar septa by a proliferation of dilated and engorged capillary channels arranged perpendicular to each other, forming a complex mesh-like framework. IFPAs, the most common of the major pulmonary

DOI: 10.1093/ajcp/aqaa156

Table 1
Clinical, Pathologic, and Radiologic Characteristics in All Patients

Characteristic	All Patients (n = 40)[a]	ALI (n = 29)	Non-ALI (n = 11)
Baseline and demographics			
Age, median (range), y	71.5 (38-97)	71.31 (38-93)	72 (57-97)
Male, No. (%)	28 (70)	20 (68.9)	8 (72.7)
Body mass index, mean (range), kg/m^2/No.	30.09 (18.93-54.7)/28	30.34 (18.93-54.7)/23	28.95 (22.42-38.1)/5
Ethnicity, No. (%)			
Hispanic	23 (57.5)	19 (65.5)	4 (36.3)
White	1 (2.5)	1 (5.2)	0 (0)
African American	2 (5)	2 (10.5)	0 (0)
Unspecified	14 (35)	7 (36.8)	7 (63.6)
SARS-CoV-2 RT-PCR, No. (%)			
Premortem diagnosis	32 (80)	26 (89.6)	6 (54.5)
Postmortem diagnosis	8 (20)	3 (10.3)	5 (45.4)
Clinical			
Comorbid Conditions, No. (%)			
Hypertension	34 (85)	23 (79.3)	11 (100)
Diabetes	20 (50)	16 (55.1)	4 (36.3)
Hyperlipidemia	15 (38.4)	10 (35.7)	5 (45.4)
Chronic heart disease	15 (37.5)	9 (31)	6 (54.5)
Chronic lung disease	10 (25)	8 (27.5)	2 (18)
Symptoms and hospital course			
Dyspnea, No. (%)/N	28 (84.8)/33	20 (90.9)/22	8 (72.7)/11
Temperature, maximum during admission (range), °C/No.	37.96 (33.9-40.9)/33	38.1 (33.9-40.9)/27	37.2 (36.3-38.5)/6
O_2 saturation at presentation, mean (No.)	80.9 (35)	81.9 (27)	77.6 (8)
Supplemental O_2, No. (%)/total No.	26 (65.0)/ 40	24 (82.8)/29	2 (18.2)/11
Time on O_2, mean (range), d	5.8 (0-25)	7.7 (0-25)	0.5 (0-5)
Received invasive mechanical ventilation or intubation, No. (%)	23 (57.5)	16 (55.2)	7 (63.6)
Admission to death, mean (range), d	10.4 (0-45)	13.2 (0-45)	3 (0-23)
Disease course (symptoms to demise), mean (range),[b] d	18 (1-40)	19.21 (1-40)	11.5 (3-23)
Medications, No. (%)			
Systemic anticoagulant	11 (27.5)	8 (27.5)	3 (27.2)
Hydroxychloroquine	20 (50)	19 (65.5)	1 (9.1)
Laboratory values, mean (range)/No.			
Platelet count, ×10^3/μL	203.93 (82-362)/33	196.11 (82-362)/27	239.16 (90-346)/6
INR on admission	1.7 (1.0-7.1)/32	1.6 (1.0-6.4)/26	2.3 (1.0-7.1)/6
D-dimer, μg/mL	10.9 (0.58-20)/26	11.4 (0.71-20)/23	7.6 (0.58-20)/3
Troponin-T, ng/L	302.5 (16-3,245)/32	225.9 (16-2,848)/27	716.2 (60-3,245)/5
NT-proBNP, pg/mL	11,956.8 (142.2-70,000)/20	13,485.2 (142.2-70,000)/16	5,843.3 (853.5-15,521)/4
IL-6, pg/mL	215.3 (36-315)/24	215 (36-315)/21	217.5 (160.2-315)/3
Pathology—macroscopic IFPA/TE, No. (%)			
Pulmonary IFPA	5 (12.5)	4 (13.7)	1 (9)
Extrapulmonary TE	5 (12.5)	1 (3.4)	4 (36.3)
Pathology—microscopic pulmonary IFPA, No. (%)			
Large organized IFPA in large vessels	19 (47.5)	16 (55.1)	3 (27.2)
Focal small IFPA	14 (35)	8 (27.5)	6 (54.5)
Diffuse small IFPA	3 (7.5)	1 (3.4)	2 (18.1)
Total IFPA	36 (90)	25 (86.2)	11 (100)
Vascular congestion and hemangiomatosis-like change	20 (50)	9 (31)	11 (100)
Imaging, No./total No. (%)			
Total patients with chest x-ray	32/40 (80.0)	26/29 (89.6)	6/11 (54.5)
Correlation of chest x-ray with pathology	30/32 (93.8)	25/26 (96.1)	5/6 (83.3)
Total patients with chest CT	3/40 (7.5)	3/29 (10.3)	0/11 (0)
Correlation of chest CT with pathology	2/3 (66.7)	2/3 (66.7)	0 (0)
Head CT—hematoma	2/5 (40)	1/3 (33.3)	1/2 (50)
Deep vein thrombosis	2/8 (25)	2/7 (28.5)	0/1 (0)
Abdominal CT—portal vein thrombosis	1/1 (100)	1/1 (100)	0/0 (0)

ALI, acute lung injury; CT, computed tomography; IFPA, intravascular fibrin or platelet-rich aggregate; IL-6, interleukin 6; INR, international normalized ratio; NT-proBNP, N-terminal prohormone of brain natriuretic peptide; RT-PCR, reverse transcription polymerase chain reaction; SARS-CoV-2, severe acute respiratory syndrome coronavirus 2; TE, thromboemboli.
[a]Complete postmortem examination with exclusion of head in some cases.
[b]Excludes patients who did or could not provide a specific history.

DOI: 10.1093/ajcp/aqaa156

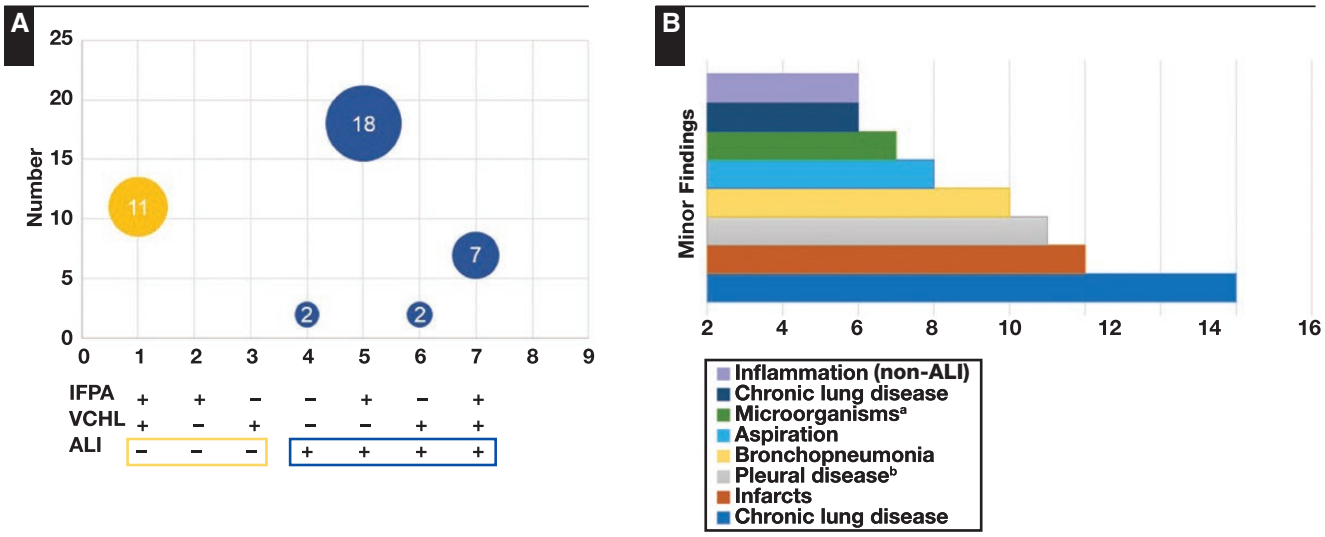

Figure 1 The spectrum of lung pathology in coronavirus disease 2019 was categorized as "major" (**A**) and "minor" (**B**) pathologic patterns. ALI, acute lung injury; IFPA, intravascular fibrin or platelet aggregate; VCHL, vascular congestion and hemangiomatosis-like change. [a]*Candida* species, herpes simplex virus, and *Aspergillus* species. [b]Congestion, fibrosis, or chronic inflammation.

findings, were large and present in either pulmonary arteries (19/40; 47.5%) or small vessels (17/40; 42.5%) and were often focal (Table 1).

Multiple minor microscopic patterns were identified, including infarcts, bronchopneumonia, aspiration, microorganisms, underlying chronic lung disease (eg, interstitial lung disease), and minimal chronic inflammation unassociated with ALI (Figure 1).

Novel and Discordant Findings

ALI, one of the three major patterns and the most commonly reported in lungs of COVID-19 decedents, was present in 29 (72.5%) of 40 cases. Eleven (27.5%) of 40 cases did not show findings of ALI—designated "non-ALI"—and were categorized as "novel." This suggested two overarching phenotypic patterns of pulmonary pathology—ALI and non-ALI—which framed subsequent analyses.

In general, there was concordance between ALI and non-ALI and the chest radiograph findings (Table 1). For the ALI group, 96% (25/26) of the patients had evidence of alveolar infiltrates, and there was evidence of disease progression for 59% (13/22), stability for 36% (8/22), and regression in 4% (1/22). For the non-ALI group, alveolar infiltrates were absent (83%; 5/6) or minimal and inconsistent with ARDS (1/6; 17%), and none (0/4) had evidence of disease progression on chest radiographs (Supplemental Table 2).

ALI vs Non-ALI: Comparison of Pathologic, Clinical and Laboratory Data, Imaging, and Cause of Death

Clinical and laboratory data and imaging findings from these two groups—ALI and non-ALI—were compared. Greater imaging and laboratory data were available for the ALI group than the non-ALI group due to the shortened interval of time from admission to death in the non-ALI group.

Patients with ALI were hospitalized longer (P = .02), were treated with supplemental oxygen longer (P = .003), and had evidence of more alveolar infiltrates on the last chest radiograph (P = .01) than the non-ALI patients (**Figure 2B** and Supplemental Figure 1). Higher radiologic grade on the last available chest radiograph significantly correlated with presence of microscopic ALI (r = 0.79, adjusted 95% confidence interval [CI], 0.29-0.95; P = .0004; **Figure 2A**). Although there was a positive trend between radiologic grade on initial chest radiography and presence of ALI, it was not statistically significant (P = .06). There was no significant association between ALI and D-dimer, troponin-T, pro-BNP, and IL-6 levels; the non-ALI decedents had limited laboratory data for similar analysis. There was no statistically significant difference in O_2 saturation at presentation, dyspnea, and T_{max} between the ALI and non-ALI patients.

The two other major patterns—IFPAs and VCHL—were evaluated in the context of ALI and "novel" non-ALI phenotypes as well as independently to assess for correlation. There was a significant negative correlation between the presence of ALI and pulmonary VCHL (r = –0.62; adjusted 95% CI, –0.87 to –0.11; P = .005; Figure 2A). No statistically significant correlation was identified between the presence of ALI and IFPAs. All non-ALI cases (11/11) had concurrent VCHL and IFPAs (Image 1B).

DOI: 10.1093/ajcp/aqaa156

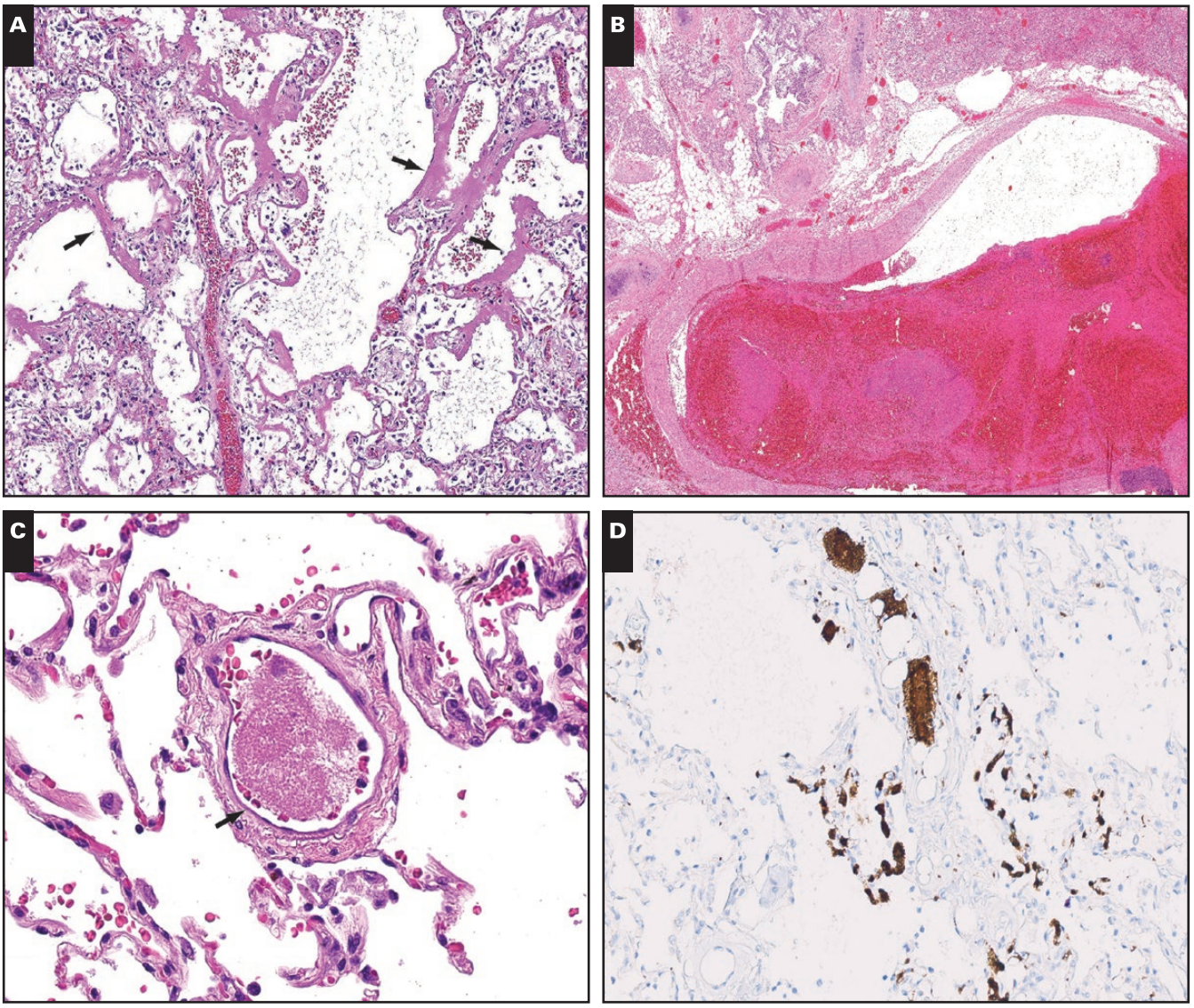

Image 1 Lung with and without acute lung injury (ALI). **A**, **B**, Lung with ALI phenotype. **A**, Eosinophilic hyaline membranes, the hallmark of diffuse alveolar damage, line alveolar septa (arrows) (H&E, ×8.3). **B**, A pulmonary artery has an organizing thrombus (H&E, ×1.2). **C**, **D**, A non-ALI phenotype. **C**, An intravascular fibrin-platelet aggregate (arrow) in a small-caliber vessel in a background of otherwise unremarkable lung parenchyma (H&E, ×40). **D**, CD61 immunohistochemical stain highlights the platelets within small vessels and capillaries of alveolar septa (×20).

Meanwhile, 27 of 29 ALI cases had IFPAs (18), VCHL (2), or both (7); two had neither VCHL nor IFPAs.

A pathologic microscopic or macroscopic cause of death was identified in only two of 11 non-ALI decedents and attributable to pulmonary thromboembolism and intracranial hemorrhage. The cause of death for the remaining nine of 11 non-ALI cases was based on adjudication of clinical and pathologic findings Table 2 and included cardiac arrest or respiratory failure in eight and septic shock in one; all had mild to moderate myocyte hypertrophy and interstitial fibrosis; seven of nine had coronary artery disease.

Controls

Review of pulmonary H&E slides from seven ALI "controls" showed large IFPAs in two cases and small, focal IFPAs in five cases. The non-ALI controls, which were from decedents who had similar median ages, sex distribution, abbreviated hospital course, comorbidities, and cause of death as the non-ALI cohort, lacked IFPAs and had focal congestion but not the accompanying hemagiomatosis-like meshwork, which was present diffusely in nine of 11 and focally in two of 11 non-ALI cases (Image 2).

DOI: 10.1093/ajcp/aqaa156

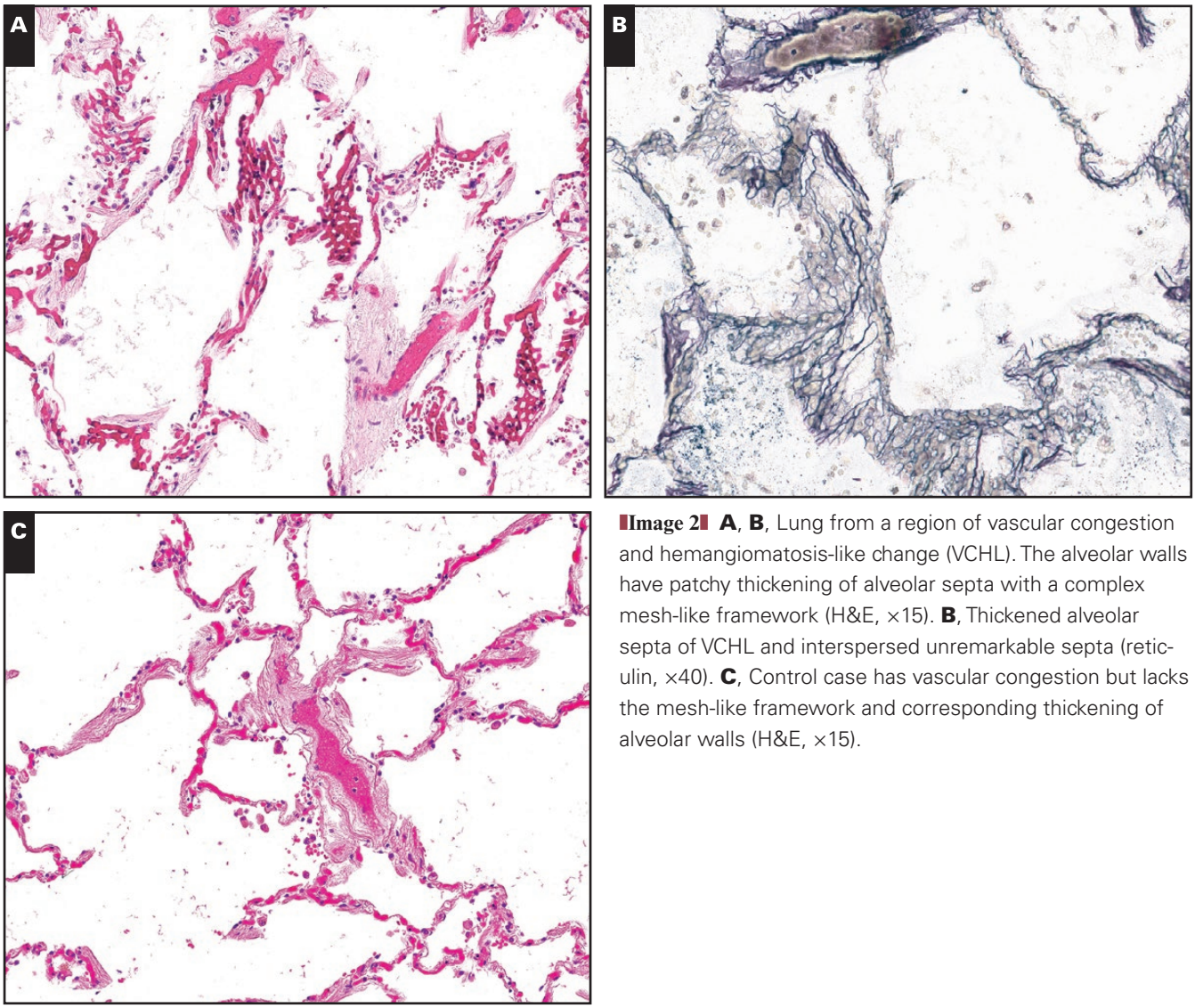

Image 2 **A**, **B**, Lung from a region of vascular congestion and hemangiomatosis-like change (VCHL). The alveolar walls have patchy thickening of alveolar septa with a complex mesh-like framework (H&E, ×15). **B**, Thickened alveolar septa of VCHL and interspersed unremarkable septa (reticulin, ×40). **C**, Control case has vascular congestion but lacks the mesh-like framework and corresponding thickening of alveolar walls (H&E, ×15).

Discussion

In our cohort, three major pulmonary patterns were identified: ALI in 29 (73%) of 40, IFPAs in 36 (90%) of 40, and VCHL in 20 (50%) of 40. Second, there was a novel finding of non-ALI, which suggested two main pulmonary pathologic phenotypes—ALI and non-ALI. Each major finding was reviewed independently and in the context of the others to assess for correlation among them.

In patients with COVID-19, DAD has been described extensively[1-3,5,7,9,12-16] and AFOP in five (83.3%) of six cases in a single small series.[11] Meanwhile, an absence of DAD (non-ALI) has been described rarely[6,11,12] and infrequently correlated with clinical or imaging findings.[12]

ALI vs Non-ALI

For these reasons, while ALI and non-ALI were evaluated in parallel for similarities and differences, the primary focus was on the non-ALI phenotype. First and foremost, the presence of the two distinct pathologically identified phenotypes was corroborated with available data. Although imaging was limited to primarily chest radiographs and performed only for a subset (n = 6) of non-ALI decedents (due in large part to early death in that cohort), the overall concordance between radiology and pathology was 93.8%, which argues against undersampling of ALI. Furthermore, when present microscopically, ALI was evident in most H&E slides (mean, 78.4%), also making undersampling an unlikely cause for its absence in the non-ALI cohort. Although it can be unevenly distributed, DAD in COVID-19 has been described bilaterally and in all lobes.[16]

Clinical, laboratory, and radiologic data were assessed for distinct patterns that correspond to the microscopically identified ALI and non-ALI phenotypes. There was no difference in O_2 saturation at presentation,

DOI: 10.1093/ajcp/aqaa156

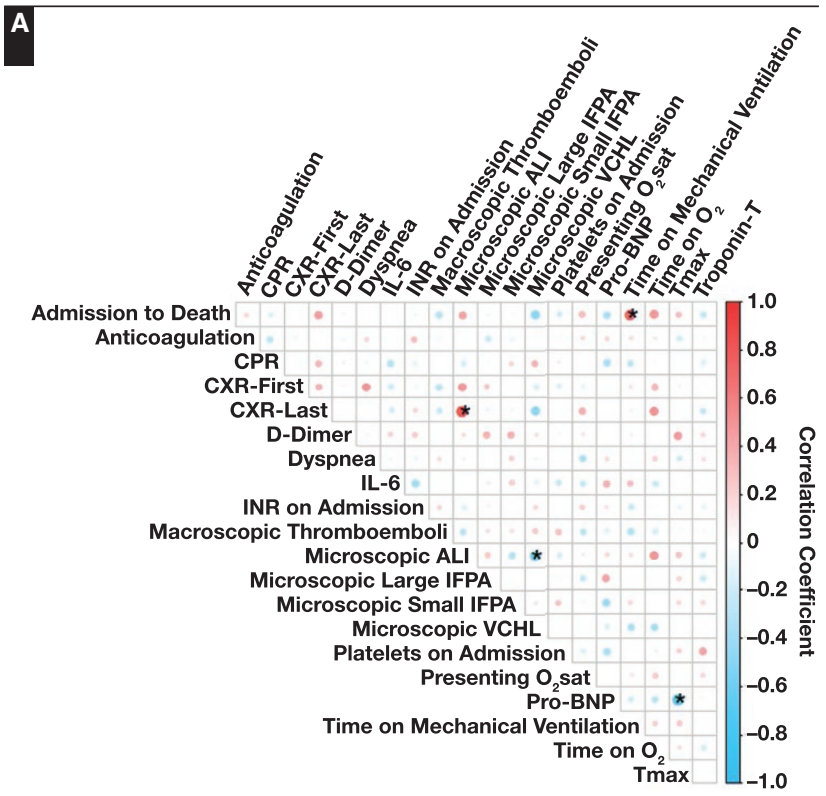

Figure 2 Associations between clinical, laboratory, radiologic, and microscopic findings. **A**, Correlation matrix of clinical, laboratory, major microscopic, and radiologic data. Circle size and color intensity are proportional to correlation coefficient, with red representing positive correlations and blue representing negative correlations. *Statistical significance (Holm-adjusted $P < .05$).

dyspnea, and T_{max} between ALI and non-ALI. There was a statistically significant difference in the length of the hospital course between ALI (mean, 13.2 days) and non-ALI (mean, 3.0 days) decedents—the latter were hospitalized, if at all, for fewer days. Radiographically, patients with ALI were significantly more likely to have higher grade findings, corresponding to consolidation, on chest radiographs compared with the non-ALI group. The abbreviated hospitalization in the non-ALI group resulted in limited clinical and laboratory data for comprehensive assessment of premortem parameters. With the exception of two cases, which showed a macroscopic pulmonary embolism or intracranial hemorrhage, a definitive pathologically confirmed cause of death for the non-ALI decedents was not identified. Neither myocarditis nor myocardial infarction, which typically causes microscopic change 4 to 12 hours following the insult,[17] was microscopically evident.

The presence of a non-ALI phenotype in our cohort and the rarity of its descriptions in the literature raise important questions. First, was mortality in these patients directly attributable to COVID-19 or an alternative cause? The cause of death in most non-ALI patients was attributed to cardiac arrest or cardiopulmonary failure. COVID-19 as the predisposing condition for cardiac arrest is plausible, explains the absence of microscopic cardiac findings, and is supported by a 10-fold increase in New York City[18] and a 52% increase in four provinces in Italy[19] in out-of-hospital cardiac arrests during the pandemic relative to similar timeframes in 2019.

Second, did the non-ALI decedents have minor microscopic pattern(s) contributing to the cause of death? They had minor findings, but these were improbable causes of death—one decedent had focal bronchopneumonia comprising less than 5% of sections; none had microorganisms or microscopically evident underlying interstitial or other predisposing lung disease. Third, is a non-ALI phenotype a precursor to ALI? While this remains a possibility, it is less likely based on the imaging and microscopic features. Most patients with ALI had consolidation on imaging at the time of presentation; only two patients with ALI demonstrated progression of disease between the first chest radiograph (no consolidation) and the last chest radiograph (marked consolidation) over a span of 27 and 29 days. Furthermore, additional microscopic features that are present in the (early) exudative phase of DAD, such as interstitial edema, were not evident. Fourth, the emergence of a second phenotype may reflect larger case

DOI: 10.1093/ajcp/aqaa156

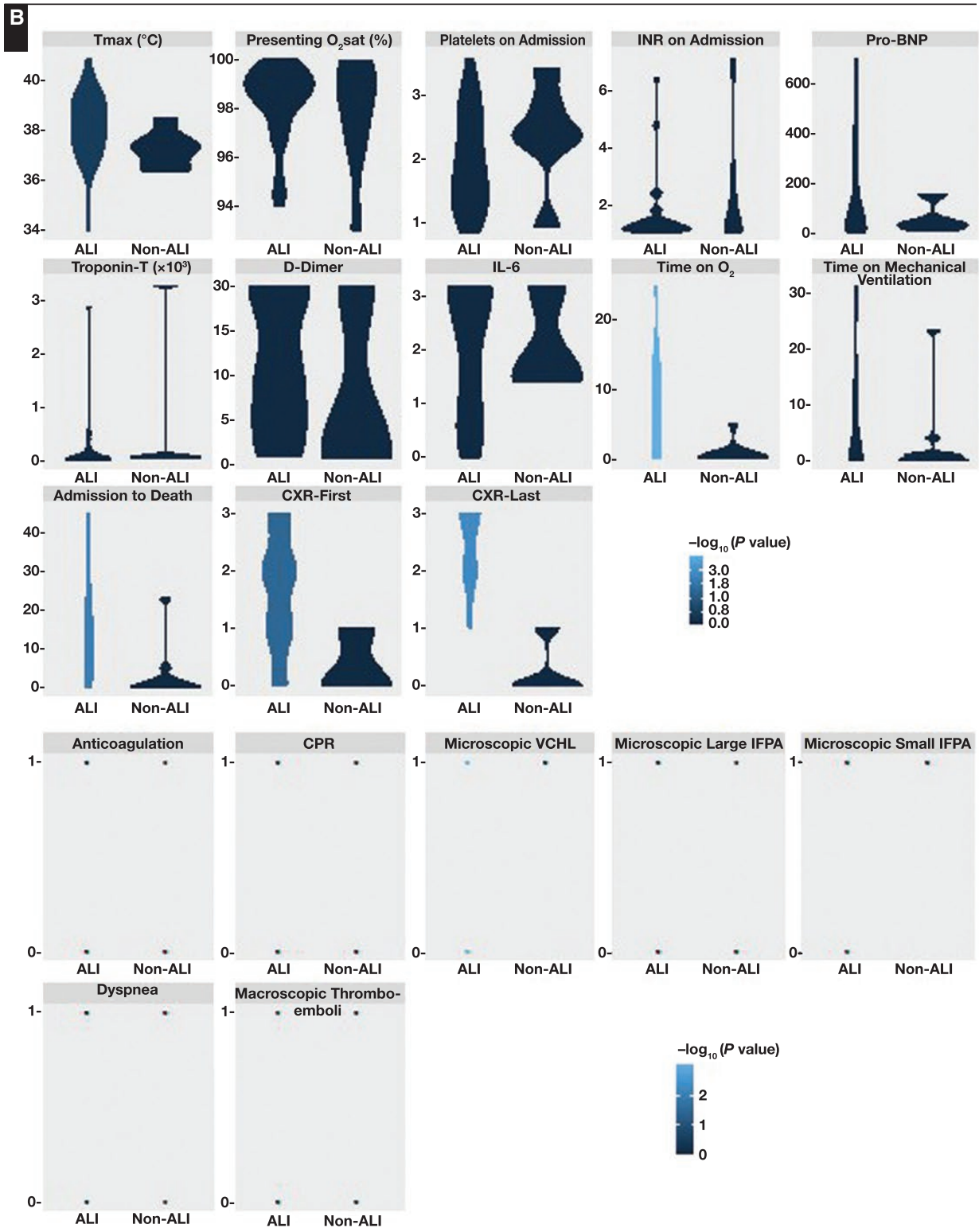

Figure 2 (cont) **B**, Violin plot and dot plots for nonbinary and binary data, respectively, of clinical, laboratory, microscopic, and radiographic data distributions by ALI status. For any given clinical feature, the violin and dot color are proportional to the $-\log_{10}$ (Holm-adjusted *P* value) of a Wilcoxon rank-sum or Fisher exact test for nonbinary and binary data, respectively, comparing the distribution of that feature in ALI vs non-ALI. Each circle corresponds to a single case. For binary data, 1 = presence, 0 = absence. ALI, acute lung injury; CPR, cardiopulmonary resuscitation; CXR, chest x-ray; IFPA, intravascular fibrin or platelet-rich aggregate; INR, international normalized ratio; pro-BNP, N-terminal prohormone of brain natriuretic peptide; Tmax, maximum temperature; VCHL, vascular congestion and hemangiomatosis-like change.

DOI: 10.1093/ajcp/aqaa156

DOI: 10.1093/ajcp/aqaa156

Table 2

Non-ALI Cohort: Clinical, Radiographic, and Pathologic Findings

	Case No.										
Characteristic	**1**	**2**	**3**	**4**	**5**	**6**	**7**	**8**	**9**	**10**	**11**
Demographics											
Sex (M = 8, F = 3)	M	M	M	F	M	M	M	M	F	F	M
Age, y (mean, 71.7; range, 57-97)	70	61	80	60	83	68	57	73	68	97	75
RT-PCR (premortem = 6/postmortem = 5)	Post	Post	Pre	Post	Pre	Pre	Post	Pre	Pre	Post	Pre
Clinical/laboratory											
Admission to death, d	0	0	1	0	2	2	0	0	23	0	5
Days on O_2, d	0	0	0	1	0	0	0	0	0	0	5
Days on ventilator, d	0	0	1	0	0	2	0	0	23	0	0
Preexisting conditions											
Hypertension	+	+	+	+	+	+	+	+	+	+	+
Diabetes	–	–	–	+	–	–	–	+	–	–	+
Cardiac disease	+	–	+	–	+	–	–	–	–	+	+
Cancer	–	–	+	–	+	–	–	–	–	+	–
Lung disease	–	–	+	–	–	–	–	–	–	–	+
Others[a]	–	–	+	+	+	+	+	–	+	+	+
Symptoms											
Fever	–	–	+	–	+	–	–	–	–	–	–
Dyspnea	+	+	–	+	+	+	–	+	+	–	+
Cough	+	–	–	–	–	–	+	–	–	–	–
Shock	–	–	+	–	–	+	–	+	+	+	–
Therapy											
Vasopressors	–	–	+	–	–	+	–	+	+	+	–
Anticoagulants	–	–	–	–	+	+	–	–	–	–	+
Steroids	–	–	–	–	–	–	–	–	+	–	–
Hydroxychloroquine	–	–	–	–	–	+	–	–	+	–	–
Antibiotics	–	–	–	–	–	+	–	+	+	–	–
Antivirals	–	–	–	–	–	–	–	–	–	–	–
Laboratory values											
D-dimer, µg/mL	NA	NA	NA	NA	NA	>20	NA	NA	1.18	NA	0.58
BNP, pg/mL	NA	NA	853	NA	15,521	NA	NA	3,710	NA	NA	11,980
Troponin-T, ng/L	NA	NA	66	NA	60	3,245	NA	0	1,520	NA	88
CRP, mg/L	NA	NA	NA	NA	NA	218.48	NA	NA	268.48	NA	89.42
Lowest SaO_2	63	NA	48	NA	79	80	NA	30	70	21	84
Lowest PaO_2	NA	NA	21	NA	NA	50	NA	22	51	NA	50
Lowest P/F	NA	NA	NA	NA	NA	236	NA	NA	248	NA	NA
Radiology											
Chest x-ray											
Volume loss	NA	NA	+	NA	+	–	NA	+	–	NA	–
Pneumothorax	NA	NA	–	NA	–	–	NA	–	–	NA	–
Pleural effusion	NA	NA	–	NA	–	–	NA	–	+	NA	+
Fibrosis	NA	NA	–	NA	–	–	NA	–	–	NA	–
Grade[b]	NA	NA	0	NA	0	0	NA	0	1	NA	0

Table 2 (cont)

Characteristic	Case No. 1	2	3	4	5	6	7	8	9	10	11
Head CT											
Hematoma	NA	NA	NA	NA	–	NA	NA	+	NA	NA	NA
Pathology											
Macroscopic findings											
Systemic TE	–	PE	–	–	–	–	Left iliac artery	Basilar artery	–	Aorta, bilateral iliac artery	Aorta
RV dilatation	–	–	–	+	–	–	+	–	+	+	–
Brain hemorrhage/infarct	–	–	–	–	–	–	–	+	–	NA	NA
Leg swelling	–	–	–	–	–	–	+	–	–	–	+
Microscopic pulmonary findings											
IFPA	+	+	+	+	+	+	+	+	+	+	+
Large IFPA	–	+	–	–	–	–	+	–	+	–	–
Small IFPA	+	+	+	+	+	+	+	+	+	+	+
VCHL	+	+	+	+	+	+	+	+	+	+	+
Aspiration	+	–	–	–	–	–	–	–	–	–	–
Chronic inflammation	+	–	–	–	–	–	–	–	+	+	+
Pulmonary infarct	–	–	+	–	–	–	–	–	–	+	
Hemorrhage	+	+	–	–	–	–	+	–	–	–	+
Bronchopneumonia	–	–	–	–	–	–	–	+	–	–	–
Microorganisms[c]	–	–	–	–	–	–	–	–	–	–	–
Pleural disease[d]	–	–	+	–	–	+	–	–	–	–	+
Emphysema	–	–	+	–	–	–	–	–	–	–	–
Organizing P (No. of slides)	–	–	–	–	–	–	–	–	Focal (1/5)	Focal (1/7)	Focal (1/7)
DAD (No. of slides)	–	–	–	–	–	–	–	–	–	–	Focal (1/7)
Fibrin (No. of slides)	Focal (1/14)	–	–	–	Focal (1/5)	–	–	–	–	–	–
Microscopic cardiac findings											
Hypertrophy	++	++	+	++	++	+	++	++	++	++	++
Fibrosis	+	+	++	+	+	+	+	+	++	++	+
Contraction bands	–	–	–	–	–	–	–	–	–	–	–
Edema	–	+	–	–	–	–	–	–	+	–	–
Myocytes damage	–	–	–	–	–	–	–	–	+	+	+
Myocarditis	–	–	–	–	–	–	–	–	–	–	–
CAD	+	++	++	+	+	++	++	+	–	+	–
Cause of death											
Cause of death[e]	Cardiac arrest	Thromboemboli	Cardiac arrest	Cardiac arrest	Septic shock	Respiratory failure/MOF	Cardiac arrest	Neurologic	Cardio-respiratory	Cardiac arrest	Cardio-respiratory
Certainty (definite or probable)	Probable	Definite	Probable	Probable	Probable	Probable	Probable	Definite	Probable	Probable	Probable

BNP, B-type natriuretic peptide; CAD, coronary artery disease; CRP, C-reactive protein; CT, computed tomography; DAD, diffuse alveolar damage; IFPA, intravascular fibrin or platelet-rich aggregate; MOF, multiorgan failure; NA, not applicable; Organizing P, organizing pneumonia; PaO_2, arterial oxygen partial pressure; PE, pulmonary embolus; P/F, arterial oxygen partial pressure/fractional inspired oxygen; RT-PCR, reverse transcription polymerase chain reaction; RV, right ventricle; SaO_2, arterial oxygen saturation; TE, thromboemboli; VCHL, vascular congestion and hemangiomatosis-like change; +, mild; ++, moderate; +++, severe; –, absent.

[a]Others = renal, dementia/neurologic disease, recent surgery, morbid obesity, hyperlipidemia.

[b]Grade (0-3): no, minimal, moderate, or marked airway opacities on last available chest x-ray. Grade 0, lung with no alveolar opacities; grade 1 (minimal): less than one-third of the lung with alveolar opacities; grade 2 (moderate), one-third to two-thirds of the lung with alveolar opacities; grade 3 (marked), more than two-thirds of the lung with alveolar opacities.

[c]Microorganisms: *Candida* species, herpes simplex virus, *Aspergillus*.

[d]Pleural disease: congestion, chronic inflammation, and/or fibrosis.

[e]The cause of death was categorized into major categories: cardiac failure, respiratory failure, cardiorespiratory failure, neurologic (eg, intracranial hemorrhage), sepsis, thromboembolic event, multiorgan failure, or unknown etiology.

numbers in our cohort. Last, the fact that this phenotype has been infrequently reported in the literature may be explained by a selection bias; in other centers, patients who were not hospitalized or only so for a short time may not have undergone postmortem examinations.

Major Microscopic Patterns

Of the three major findings, microscopic VCHL was the least common. VCHL was present in all cases of non-ALI, while it negatively correlated with ALI. Vascular congestion has been described in conjunction[14] with and without DAD[6,14] in a minority of lungs from patients with COVID-19. Relative to the images accompanying published reports, the extent of vascular congestion and accompanying alveolar wall thickening with hemangiomatosis-like change in our cohort was more prominent (Image 2). Angiogenesis has been seen in lungs of patients with COVID-19 in association with DAD.[15] The presence of thickened alveolar septa and congested capillary channels resembling a hemangiomatosis-like proliferation in our cases could be ascribed to a similar angiogenesis-type process. Other possibilities remain, such as microscopic IFPAs resulting in secondary capillary proliferation.

Overall, pulmonary IFPAs, small and large, represented the most common (90%) of the three microscopic patterns. There was no statistical correlation between the type of IFPAs (macroscopic or microscopic; pulmonary or extrapulmonary) and ALI or non-ALI phenotype. Increased macroscopic venous thromboemboli[12] and microscopic fibrin (thrombi)[7,10,13,14] have been detected in decedents with COVID-19. With the aid of ancillary studies, significantly greater numbers[15] of thrombi have been identified in lungs infected with COVID-19 relative to those with H1N1. Compared with the control cases, the COVID-19 lungs did not have increased IFPAs; however, our number of controls was relatively small and quantitated only on H&E stain. Similar to the identification of a non-ALI pattern, a key question is whether IFPAs are a manifestation of COVID-19 or related to other underlying comorbidities.

Macroscopic and microscopic pulmonary thrombi are well described in the DAD pathology literature. DAD, which is the histologic pattern ascribed to multiple possible etiologies with infection representing one, causes injury to the alveolar-capillary barrier and initiates multiple downstream effects, including proinflammatory and procoagulation pathways. In fact, fibrinogen and complement, among other proteins and cellular debris, are present in hyaline membranes of DAD,[20] and thromboemboli have been identified in 95% of lungs from 22 postmortem non–COVID-19 examinations using specimen arteriography,[21] as well as in our pre–COVID-19 postmortem controls. Therefore, pulmonary IFPAs may at least to some extent be a consequence of DAD than injury resulting from COVID-19 alone.

Nevertheless, COVID-19 as a culprit of IFPAs—either emboli or thrombi—remains a possibility, since all decedents without DAD/ALI in our study also had IFPAs. In their examination of COVID-19 cases without significant DAD, Magro et al[10] noted fibrin deposits in the microvasculature of the lung and skin and suggested activation of complement pathways. Wichmann et al[12] identified deep venous thrombosis (DVT) in both lower extremities in seven (58.3%) of 12 postmortem examinations of COVID-19 cases; six of these patients had DAD. Relatively small numbers of DVTs identified in other postmortem series, including ours, may reflect differences in prosection practice—rigorous search for DVTs in all cases vs only those with indicators on external examination. It remains to be determined if IFPAs represent thrombi or emboli. Most important, understanding the etiology of IFPAs has the potential to affect clinical management since in some scenarios, such as DAD, patients do no typically receive systemic anticoagulation. Three of five ALI decedents had macroscopic pulmonary or extrapulmonary IFPAs on systemic anticoagulation (Supplemental Table 3).

COVID-19: Mechanisms of Decompensation

Our findings support two phenotypes—ALI and non-ALI. In contrast to non-ALI, ALI is concordant with the literature and expected clinically. Non-ALI probes the understanding of COVID-19, including if it is related to COVID-19. Our data support that COVID-19 presents with primarily pulmonary, cardiac, or vascular manifestations **Figure 3**. Cardiac arrest is a consideration based upon no or minimal hospitalization, absence of microscopic changes, and the recently reported significant[18,19] increases in out-of-hospital cardiac deaths during the pandemic. The coexistence of VCHL and IFPAs in all (11/11) non-ALI cases (and only 7/29 ALI cases) suggests, rather than a nonspecific postmortem feature, the non-ALI phenotype is associated with COVID-19 infection. IFPAs raise the possibilities of microemboli from undetected DVTs, microthrombi in the pulmonary vasculature, and microthrombi secondary to coagulopathies that accompany infections. Interestingly, while the cause of death may be attributable to one or more of the above conditions, there were no significant differences in clinical parameters, such as O_2 saturation at presentation, dyspnea, and T_{max}, between the ALI and non-ALI patients. Understanding the specific mechanism(s) may potentially alter clinical management.

Conclusion

Three major pathology patterns and two distinct phenotypes were noted at autopsy, one characterized by ALI and the other without. The patients with a non-ALI phenotype represent a rarely described subgroup. The cause of death in this subset may include

DOI: 10.1093/ajcp/aqaa156

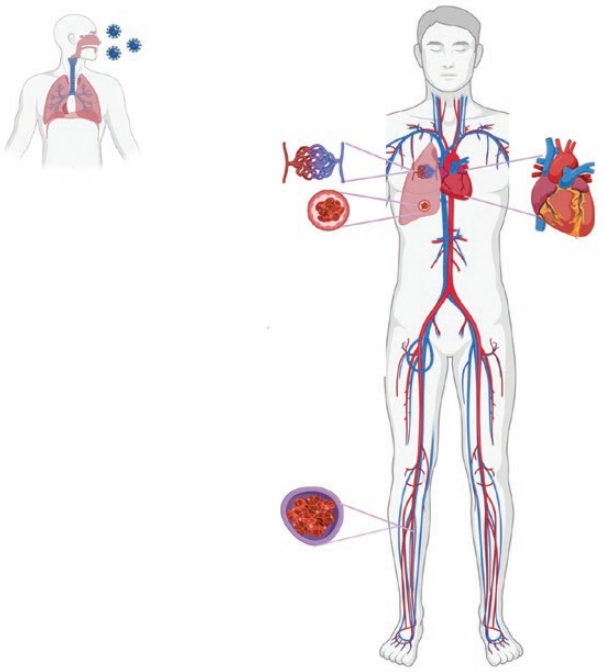

Figure 3 Potential mechanisms of decompensation in non–acute lung injury phenotype that include a vascular or cardiac pathway.

cardiac and/or vascular pathways and requires additional corroboration.

Corresponding author: Anjali Saqi, MD, MBA; aas177@cumc.columbia.edu.
**First authors.*

References

1. Barton LM, Duval EJ, Stroberg E, et al. COVID-19 autopsies, Oklahoma, USA. *Am J Clin Pathol.* 2020;153:725-733.
2. Xu Z, Shi L, Wang Y, et al. Pathological findings of COVID-19 associated with acute respiratory distress syndrome. *Lancet Respir Med.* 2020;8:420-422.
3. Zhang H, Zhou P, Wei Y, et al. Histopathologic changes and SARS-CoV-2 immunostaining in the lung of a patient with COVID-19. *Ann Intern Med.* 2020;172:629-632.
4. Pernazza A, Mancini M, Rullo E, et al. Early histologic findings of pulmonary SARS-CoV-2 infection detected in a surgical specimen [published online April 30, 2020]. *Virchows Arch.*
5. Konopka KE, Wilson A, Myers JL. Postmortem lung findings in an asthmatic patient with coronavirus disease 2019 [published online April 28, 2020]. *Chest.*
6. Varga Z, Flammer AJ, Steiger P, et al. Endothelial cell infection and endotheliitis in COVID-19. *Lancet.* 2020;395:1417-1418.
7. Fox S, Akmatbekov A, Harbert JL, et al. Pulmonary and cardiac pathology in Covid-19: the first autopsy series from New Orleans. *medRxiv.* 2020. doi: 10.1101/2020.04.06.20050575.
8. Tian S, Hu W, Niu L, et al. Pulmonary pathology of early-phase 2019 novel coronavirus (COVID-19) pneumonia in two patients with lung cancer. *J Thorac Oncol.* 2020;15:700-704.
9. Tian S, Xiong Y, Liu H, et al. Pathological study of the 2019 novel coronavirus disease (COVID-19) through postmortem core biopsies. *Mod Pathol.* 2020;33:1007-1014.
10. Magro C, Mulvey JJ, Berlin D, et al. Complement associated microvascular injury and thrombosis in the pathogenesis of severe COVID-19 infection: a report of five cases. *Transl Res.* 2020;220:1-13.
11. Copin MC, Parmentier E, Duburcq T, et al. Time to consider histologic pattern of lung injury to treat critically ill patients with COVID-19 infection [published online April 23, 2020]. *Intensive Care Med.*
12. Wichmann D, Sperhake JP, Lutgehetmann M, et al. Autopsy findings and venous thromboembolism in patients with COVID-19: a prospective cohort study [published online May 6, 2020]. *Ann Intern Med.* 2020.
13. Carsana LS, Sonzogni A, Nasr A, et al. Pulmonary post-mortem findings in a large series of COVID-19 cases from Northern Italy [published online June 8, 2020]. *Lancet Infect Dis.*
14. Menter T, Haslbauer JD, Nienhold R, et al. Post-mortem examination of COVID19 patients reveals diffuse alveolar damage with severe capillary congestion and variegated findings of lungs and other organs suggesting vascular dysfunction [published online May 4, 2020]. *Histopathology.*
15. Ackermann M, Verleden SE, Kuehnel M, et al. Pulmonary vascular endothelialitis, thrombosis, and angiogenesis in Covid-19. *N Engl J Med.* 2020;383-120-128.
16. Schaller T, Hirschbuhl K, Burkhardt K, et al. Postmortem examination of patients with COVID-19. *JAMA.* 2020;323:2518-2520.
17. Kumar V, Abbas AK, Aster JC. *Robbins and Cotran Pathologic Basis of Disease.* 9th ed. Philadelphia, PA: Elsevier Saunders; 2014.
18. Lai PH, Lancet EA, Weiden MD, et al. Characteristics associated with out-of-hospital cardiac arrests and resuscitations during the novel coronavirus disease 2019 pandemic in New York City [published online June 19, 2020]. *JAMA Cardiol.*
19. Baldi E, Sechi GM, Mare C, et al. COVID-19 kills at home: the close relationship between the epidemic and the increase of out-of-hospital cardiac arrests [published online June 20, 2020]. *Eur Heart J.* 2020.
20. Tomashefski JF Jr, Cagle PT, Farver CF, et al. *Dail and Hammar's Pulmonary Pathology: Vol. 1. Nonneoplastic Lung Disease.* 3rd ed. New York, NY: Springer; 2008.
21. Tomashefski JF Jr, Davies P, Boggis C, et al. The pulmonary vascular lesions of the adult respiratory distress syndrome. *Am J Pathol.* 1983;112:112-126.

DOI: 10.1093/ajcp/aqaa156